Advanced Review

Magnetic quantum dots for multimodal imaging

Rolf Koole,[1]* Willem J. M. Mulder,[2] Matti M. van Schooneveld,[1] Gustav J. Strijkers,[3] Andries Meijerink[1] and Klaas Nicolay[3]

Multimodal contrast agents based on highly luminescent quantum dots (QDs) combined with magnetic nanoparticles (MNPs) or ions form an exciting class of new materials for bioimaging. With two functionalities integrated in a single nanoparticle, a sensitive contrast agent for two very powerful and highly complementary imaging techniques [fluorescence imaging and magnetic resonance imaging (MRI)] is obtained. In this review, the state of the art in this rapidly developing field is given. This is done by describing the developments for four different approaches to integrate the fluorescence and magnetic properties in a single nanoparticle. The first type of particles is created by the growth of heterostructures in which a QD is either overgrown with a layer of a magnetic material or linked to a (superpara, or ferro) MNP. The second approach involves doping of paramagnetic ions into QDs. A third option is to use silica or polymer nanoparticles as a matrix for the incorporation of both QDs and MNPs. Finally, it is possible to introduce chelating molecules with paramagnetic ions (e.g., Gd-DTPA) into the coordination shell of the QDs. All different approaches have resulted in recent breakthroughs and the demonstration of the capability of bioimaging using both functionalities. In addition to giving an overview of the most exciting recent developments, the pros and cons of the four different classes of bimodal contrast agents are discussed, ending with an outlook on the future of this emerging new field. *WIREs Nanomed Nanobiotechnol* 2009 1 475–491

One of the most rapidly developing and exciting applications of nanotechnology in biomedical research is the use of nanosized semiconductor materials for (*in vivo*) imaging. These nanosized semiconductor materials, also known as quantum dots (QDs), exhibit a number of exceptional optical properties, which greatly enhance the potential of fluorescence-based bioimaging. The most significant properties include (1) a high quantum yield; (2) broad absorption with narrow, symmetric photoluminescence spectra; and (3) a high resistance to photobleaching and chemical degradation. In addition, surface chemistry of QDs allows the inclusion of entities for improved pharmacokinetics and bioapplicability, and the conjugation of specific targeting molecules. Since the early studies describing the first biological application of QDs as fluorescent biological labels appeared in the late 1990s, the field has revolutionized.[1,2] These studies demonstrate the use of QDs for labeling cultured cells, and since the publication of phospholipid micelle–coated QDs, for *in vivo* imaging,[3] numerous studies exploit their unique fluorescent properties for the same purpose. Gao et al. used QDs for *in vivo* cancer targeting and imaging,[4] while Stroh et al. used multiphoton microscopy techniques combined with the application of QD preparations to spectrally distinguish multiple species within the tumor milieu *in vivo*.[5] In addition to the above-mentioned applications in cell labeling and targeting for *in vitro* and *in vivo* imaging, QDs have also been employed as biosensors. For example, Medintz and colleagues have designed a QD protein conjugate that functions as a sugar sensor.[6] This conjugate can be used to monitor the competition between

*Correspondence to: r.koole@uu.nl

[1]Condensed Matter and Interfaces, Debye Institute, University Utrecht, The Netherlands.

[2]Sinai Translational and Molecular Imaging Institute and Imaging Science Laboratories, Mount Sinai School of Medicine, New York, USA.

[3]Biomedical NMR, Biomedical Engineering, Eindhoven University of Technology, The Netherlands.

DOI: 10.1002/wnan.014

cyclodextrin and maltose in binding to receptor proteins attached to the QDs. Another example of how surface modification can contribute to extending the applicability of QDs was demonstrated by So et al. They created self-illuminating QDs by conjugation of a mutant of the bioluminescent protein Renilla reniformis luciferase to the surface of QDs.[7] When this protein binds its substrate coelenterazine, it emits blue light, which can excite the bound QD, resulting in QD emission.

All the aforementioned examples demonstrate the broad range of exciting possibilities QDs exhibit as optical biolabels. Interestingly, new developments in nanochemistry allow for the creation of QD-based nanoparticulate materials that can also be detected with other imaging techniques, the so-called multimodal QDs. Recently, the combination of QDs with a radiolabel has shown to be valuable for the *in vivo* investigation of the pharmacokinetics and biodistribution of QDs with positron emission tomography (PET) imaging.[8] As another example, it was recently shown that QDs (even without modification) can be detected by computed tomography (CT) because of the high electron density of QD cores.[9] Furthermore, QDs can be designed such that they also display (super)paramagnetic properties for their detection with magnetic resonance imaging (MRI). MRI is a diagnostic tool that is characterized by its ability to generate three-dimensional images of opaque and soft tissue with relatively high spatial resolution and tissue contrast, and therefore is the most versatile imaging technique available in the clinic. Apart from anatomical information, metabolic and functional parameters can also be obtained with MRI. Contrast agents are currently applied in 30 to 40% of clinical MRI scans. Nanoparticulate MRI contrast agents, utilized primarily for molecular imaging purposes, have been developed since the mid-1990s. Due to the complementary characteristics of optical techniques and MRI, combinatory probes, which exhibit both fluorescent and (super)paramagnetic properties, offer significant advantages. Recently, several research groups have started developing (super)paramagnetic QDs for this purpose. Several strategies to accomplish this may be employed. In this review we will discuss (1) core/shell and heterostructures of magnetic materials and QDs, (2) QDs doped with paramagnetic ions, (3) composite nanostructures combining magnetic particles and QDs, and (4) QDs with a paramagnetic coating of Gd-chelates. In addition to examining their design and characteristics, we will review their application *in vitro* and, where possible, *in vivo*.

INTRODUCTION TO QUANTUM DOTS AND MAGNETIC RESONANCE IMAGING CONTRAST AGENTS

Semiconductor nanoparticles that are smaller than the spatial extension of electrons and holes in the bulk semiconductor show quantum-size effects and are called QDs. These effects typically occur in the 1–10-nm size regime. Because of the very small size of the box available, the (kinetic) energy of the electrons and holes increases with decreasing particle size, causing an increase in the energy difference between the conduction and the valence band (i.e., an increase in the bandgap). This results in strongly size-dependent absorption and emission spectra for QDs, both shifting to higher energies for decreasing particle size. The emission originates from the lowest exciton (electron–hole pair) state and is narrow. The absorption spectrum is broad owing to the energetic width of the conduction and valence bands, and the QD fluorescence can therefore be excited over a broad spectral range.

The small size also allows luminescence quantum efficiencies (QE) that are much higher than for bulk semiconductors. QE is defined as the number of photons emitted divided by the number of photons absorbed. Because of the confinement of the electrons and holes and the possibility to synthesize defect-free QDs, the chance that an electron or hole is trapped by a defect (resulting in recombination without the emission of light) is much smaller in a QD as compared to bulk semiconductors. If the nanocrystal surface is correctly passivated (no surface quenching states), the exciton created upon absorption has no choice but to recombine radiatively (emitting a photon) giving rise to a high QE (up to 80%).

A crucial step to improve the QE and stability of QDs involves the growth of a shell of a wider bandgap material around the QD core. The wider bandgap shell confines the electron and holes to the core and reduces surface reactions with, e.g., oxygen and thereby increases the stability against photoxidation. Ideally, the shell material is lattice-matched with that of the core to prevent interfacial defects that can reduce the QE. The improved stability of these so-called core/shell QDs not only gives a long shelf life (years under ambient conditions) but also provides a superior bleaching behavior. The number of photons emitted before the QD is bleached is 3 orders of magnitude higher than for fluorescent dye molecules. It is for the unique properties of QDs outlined above that they are very promising as labels for fluorescence imaging.

Most MRI contrast agents generate contrast by locally shortening the ^{1}H relaxation times of

the surrounding water.[10] Relaxation is the process describing a return to thermal equilibrium of protons in a magnetic field, which were initially excited by the application of a radio frequency magnetic field pulse in the MRI scanner. The relaxation is usually divided into two principal relaxation processes: spin–lattice or longitudinal relaxation (characteristic time T_1 [s] or relaxation rate R_1 [s^{-1}]) and spin–spin or transverse relaxation (T_2, R_2). The transverse relaxation process may be accelerated by magnetic field inhomogeneities, in which case the relaxation process is referred to as T_2*. For reasons of simplicity we will refer only to T_2 in the rest of this review, but it should be taken into consideration that in case T_2 is mentioned we also refer to T_2*. The MR scanner can be made sensitive to differences and changes in the relaxation times by appropriately tuning the MRI sequences. T_1-weighted MR sequences produce images in which areas with low T_1 are bright (positive contrast), while T_2-weighted MR sequences result in images with dark areas of low T_2 (negative contrast).

The ability of a contrast agent to accelerate relaxation is defined by the change in relaxation rate per unit concentration of the contrast agent. The proportionality constants are denoted as r_1 and r_2 (units [mM^{-1} s^{-1}]), where $r_2 \geqslant r_1$. Since T_1 and T_2 relaxation are not completely independent processes, a contrast agent is never exclusively a positive or negative contrast agent. In practice, the ratio between r_2 and r_1 determines whether a contrast agent is more suitable for T_1-weighted positive contrast imaging or for T_2-weighted negative contrast. As a rule of thumb, agents with an r_2/r_1 between 1 and 2 are most suitable as T_1 contrast agents, while contrast agents with larger r_2/r_1 ratio become progressively more suitable for T_2-weighted imaging.

T_1 contrast agents are commonly paramagnetic metal ions (e.g., Gd^{3+}) coordinated to a protective chelate to form a nontoxic complex.[11] The principal action of the agent is electron–proton dipolar coupling, which falls off rapidly with distance. This means that water should be directly coordinated to the paramagnetic ion for effective relaxation and preferably should undergo fast water exchange. Slowing down the rotational motion of the complex, for example, by attaching the contrast agent to a nanoparticle, results in improved relaxation.

The most effective way to decrease T_2 is to use agents that are generally classified as superparamagnetic contrast agents.[12] These are typically iron oxide nanoparticles composed of magnetite (Fe_3O_4) or maghemite (γ-Fe_2O_3).[13] Local field inhomogeneities surrounding the magnetic particles lead to rapid dephasing of transverse magnetization and therefore a short T_2 relaxation time. Above the so-called blocking temperature (T_b), these nanoparticles are superparamagnetic because the magnetocrystalline anisotropy is overcome by temperature fluctuations, causing the magnetic moment to randomly change directions within the particle. Inversely, these particles are ferromagnetic below T_b. The magnetic field required to reduce the magnetization to zero after the particle has been fully magnetized is called the coercivity. We refer the reader to a cross-reference (see the end of the paper) for more details on the magnetic properties of iron oxide nanoparticles.

Core/Shell and Heterostructures (Type I)

This section discusses the nanocrystals that resemble the structure denoted as Type I in Figure 1, in which the magnetic nanoparticle (MNP) and QD are fused together to form either a core/shell or heterostructure. Despite the generally large lattice mismatch between magnetic and semiconductor nanocrystals, it has recently been shown that it is possible to combine the two materials within one nanocrystal, although the mechanism of attachment has not been fully resolved yet.[14] The four examples discussed below are all synthesized using a wet chemical procedure, in which the magnetic core is synthesized prior to the attachment of the semiconductor material (i.e., the QD). Typically, a mixture of noncoordinating (e.g., octyl ether or phenyl ether) and coordinating solvents (e.g., trioctylphosphine or oleyl amine) is used, to which the metal (e.g., $Fe(CO)_5$ or $Cd(Me)_2$) and chalcogen precursors (e.g., sulfur powder or trioctylphosphine–selenium complexes) are added.

The combination of superparamagnetic FePt NPs with CdSe or CdS QDs was studied by two different groups, showing that both core/shell (Figure 2(a), Type Ia) and heterostructures (Figure 2(b), Type Ib) can be synthesized.[15,16] Gao et al. reported the synthesis of FePt cores with a diameter of ~3 nm, surrounded by a 3–5 nm CdSe shell[15] (Figure 2(a)). In addition to CdSe, the authors show that it is possible to coat the FePt cores with a CdS or CdTe shell. FePt/CdSe core/shell nanocrystals displayed a fluorescence emission around 465 nm, which is not expected on the basis of the large volume of the CdSe shell. The authors attribute the blue emission to smaller domains of approximately 2 nm that make up the CdSe shell. The FePt/CdSe nanocrystals exhibited a fluorescence QE of 7–10%, which was low compared to that of CdSe QDs alone. The luminescence quenching was ascribed to an interaction of the QD with the metallic core, but this was not investigated in detail. The superparamagnetic properties of the FePt cores were maintained,

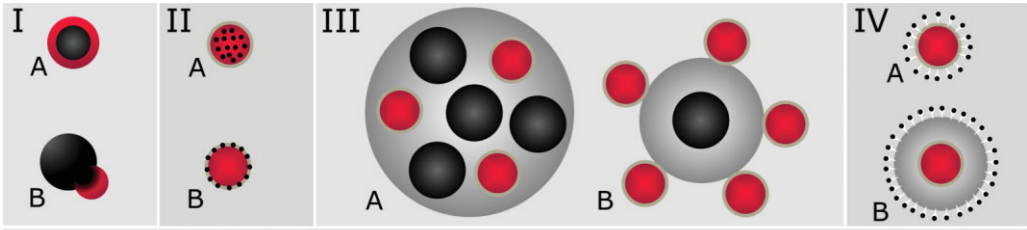

	Type	Examples
I	**Core/shell** and **heterostructures** of magnetic and semiconductor materials	-References: 14, 15, 16, 17
II	Semiconductor nanoparticles **doped** with **paramagnetic ions**	-References: 25, 27, 28, 30, 31, 34, 35, 36, 37
III	**Composite particles** combining magnetic and semiconductor nanoparticles	-References: 39, 40, 41, 44, 49, 50, 51, 52, 53, 54
IV	Semiconductor nanoparticles with a **paramagnetic coating** of **Gd-chelates**	-References: 18, 61, 63, 64, 65

FIGURE 1 | Schematic representation of the four types of magnetic quantum dots (QDs) that are discussed.

derived from the low blocking temperature of 14 K that was determined for the core/shell particles. In a similar fashion, Gu and coworkers showed the formation of FePt–CdS heterodimers[16] (Figure 2(b)). They suggest that the initial FePt/CdS core/shell structure was transformed into a heterodimer upon heating. The final particle was smaller than 10 nm, consisting of FePt and CdS nanocrystals of 2.5 and 3.5 nm, respectively. In this case, the fluorescence emission peak at 438 nm was consistent with CdS QDs of a similar size, and the heterodimers had a QE of 3%. The particles were superparamagnetic, with a blocking temperature of 11 K and coercivity (H_c) of 0.85 kOe (at 5 K).

A different class of core/shell structures, reported by Kim et al., consisted of a superparamagnetic cobalt core surrounded by a CdSe shell.[17] In contrast to the one-pot synthesis discussed above, the cobalt particles were first precipitated and redispersed in a coordinating solvent prior to the addition of the CdSe precursor materials. The cobalt cores of the final particles were 8 nm in diameter, with a CdSe shell of 2 nm (Figure 2(c)). The fluorescence emission peak of the Co/CdSe core/shell particles was located around 580 nm with a Stokes shift of 40–50 nm, which is large compared to common CdSe QDs. Interestingly, the QE of these particles (2–3%) increased with decreasing temperature, together with an increase in the radiative decay rate. These observations are unusual for CdSe QDs, and it was suggested by the authors that an interaction of the QD with the magnetic core might have modified the spin structure of the lowest excitonic state, accelerating the radiative decay. The blocking temperature of 350 K for the cobalt cores decreased to 240 K for the core/shell particles, together with a significant decrease in saturation magnetization per gram. These changes in magnetic properties were attributed to the

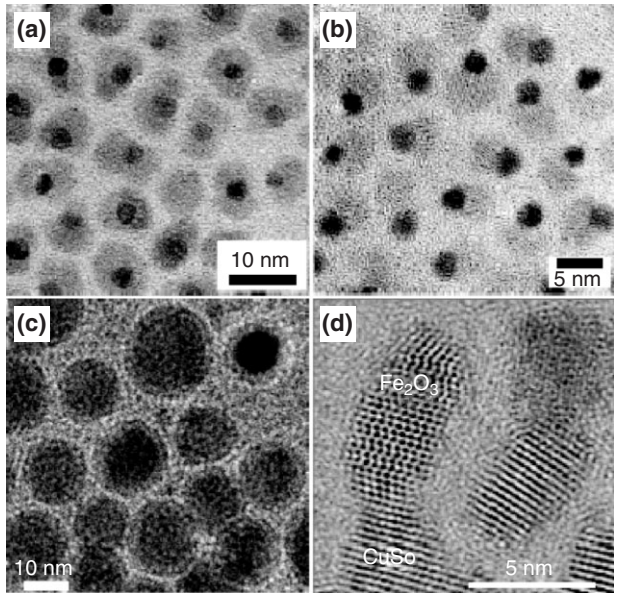

FIGURE 2 | Transmission Electron Microscopy (TEM) images of (a) FePt/CdSe core/shell nanocrystals, reprinted with permission from Ref. 15. Copyright (2007) American Chemical Society. (b) FePt–CdS heterodimers, reprinted with permission from Ref. 16. Copyright (2004) American Chemical Society. (c) Cobalt/CdSe core/shell nanocrystals, reprinted with permission from Ref. 17. Copyright (2007) American Chemical Society. (d) HR-TEM image of Fe_2O_3–CdSe heterodimers. The magnetic materials (FePt and Co) exhibit a stronger contrast in the TEM images than the semiconductor materials (CdSe and CdS). (Reprinted, with permission, from Ref. 18. Copyright 2007 Wiley-VCH Verlag GmbH & Co. KGaA.)

presence of the nonmagnetic CdSe phase. In contrast, the coercivity of the particles (0.11 T or 1.1 kOe) did not change after the CdSe coating.

The final example of a heterodimer containing a magnetic and semiconductor nanoparticle was reported by Selvan and coworkers.[18] In this case, CdSe QDs were attached to preformed superparamagnetic Fe_2O_3 MNPs (Figure 2(d)). A detailed study on the attachment mechanism of CdS QDs to Fe_2O_3 NPs was reported by another group.[14] The yield of heterodimers relative to single QDs after synthesis was high, as can be deducted from Figure 3(a). In case the suspension containing the particles was exposed to a permanent magnetic field, all the particles were attracted towards the magnet, leaving behind a clear solution. The Fe_2O_3 core was 8–10 nm in diameter, and the size of the QD could be varied between 2 and 5 nm by simply changing the reaction time. As a consequence, the emission color of the QDs could be varied between 550 and 600nm, as is illustrated in Figure 3(b). The QE of the final heterodimers was 13–18%, which is high compared to the examples discussed above. The authors do not discuss the magnetic properties of the Fe_2O_3–CdSe nanodimers in detail, although it is mentioned that they exhibit superparamagnetism. For biological applications, the heterodimers were rendered water soluble by first coating the NPs by a thin silica shell, using a reverse micelle approach. The silica particles were amine-functionalized using an amine–silane precursor (3-aminopropyl-trimethoxysilane, APS), which allowed the attachment of biofunctional groups through a covalent amide bond. In this case, the authors attached oleyl-PEG-hydroxysuccinimide groups to the silanized heterodimers, which effectively targets the particles to cell membranes. An *in vitro* study confirmed the successful biofunctionalization of the silanized heterodimers using 4T1 mouse breast cancer cells[18] (Figure 3(c)).

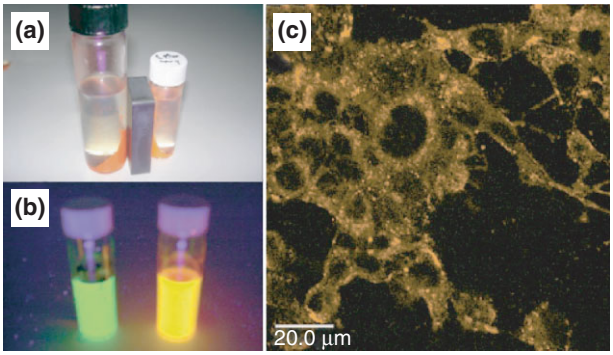

FIGURE 3 | Photographs of dispersions of various Fe_2O_3–CdSe heterodimer samples (as shown in Figure 2D). (A) shows that all particles are attracted by a magnet leaving behind a clear solution, and (B) illustrates the tunability of the emission color, by exciting two samples with a UV lamp (365 nm). (C) Confocal laser scanning microscopy of 4T1 mouse breast tumor cells incubated with oleyl-PEG coated Fe_2O_3–CdSe heterodimers. (Reprinted, with permission, from Ref. 18 Copyright 2007 Wiley-VCH Verlag GmbH & Co. KGaA.)

In summary, the core/shell and heterostructures discussed above are typically around 10 nm in size, and show both superparamagnetic and fluorescent properties. The QE of the QDs is generally low using this approach, which is probably caused by an interaction with the magnetic particle (causing emission quenching) and may therefore be an intrinsic problem of this architecture. Although biofunctionalization of these particles was shown only for the last example, it may be assumed that the core/shell and heterostructures can be rendered bioapplicable using the different methods reported in literature for hydrophobic nanoparticles. Examples are the incorporation of NPs in micelles,[3,19] coating the NPs with functionalized molecules using a ligand exchange,[20–22] or coating the NPs with a thin silica shell.[2,23]

Doped Quantum Dots (Type II)

Doping paramagnetic luminescent ions into QDs provides a direct method to incorporate fluorescence and magnetic properties into a single nanoparticle. There is a long tradition of doping paramagnetic ions into semiconductors.[24] Paramagnetic ions that have energy states within the QD bandgap introduce 'trap' states that determine the wavelength and lifetime of the doped QD luminescence. The luminescence may originate from the paramagnetic ion itself (for example, an intraconfigurational $3d^n$ transition), or involve recombination to bandgap states related to the paramagnetic dopant. Research on QDs doped with (paramagnetic) transition-metal ions rapidly increased after an early report in 1994, in which a high luminescence quantum yield and a spectacular shortening of the luminescence life time was observed for $ZnS:Mn^{2+}$ nanocrystals.[25] Later research demonstrated that the reported lifetime shortening was incorrect;[26,27] nevertheless, an entire new field had opened. Since then, many new and interesting phenomena and applications have been reported for doped QDs, including studies on the use of doped QDs as multifunctional probes for bioimaging.

An important aspect is the actual incorporation of the dopant ions into the semiconductor core. It is not trivial to provide evidence for the dopant being inside the semiconductor particle and not absorbed on

the outside of the particle. Spectroscopic techniques such as luminescence spectroscopy, electron paramagnetic resonance (EPR), and X-rays spectroscopy (e.g., extended X-ray absorption fine structure (EXAFS)) have been applied to verify the location of the dopant ions and have shown that whether incorporation of the dopant occurs depends critically on the synthesis method.[28] Basically, four types of methods are used to synthesize doped QDs. The most straighforward method involves the growth of semiconductor QDs in a solution of precursors for the semiconductor QD and the dopant ion, in the presence of a passivating ligand. As the semiconductor nanocrystal grows within the shell of coordinating ligands, some dopant ions are incorporated, provided that they are chemically similar to the semiconductor cation. Examples of the successful preparation of doped QDs using this method are the synthesis of the widely studied $ZnS:Mn^{2+}$ and $ZnO:Co^{2+}$ QDs.[26,28,29] An alternative method involves the use of an inverse micelle solution in which the QDs grow inside water droplets from precursors dissolved in the water phase.[28] The well-known hot injection method for the synthesis of undoped QDs[30] can also be modified by including a dopant precursor in the reaction mixture. For $ZnSe:Mn^{2+}$, this method proved to be successful.[31,32] However, for $CdSe:Mn^{2+}$ QDs, it was demonstrated that Mn^{2+} cannot be incorporated by the hot injection method and this was suggested to be related to the crystal structure of CdSe.[33] Incorporation of Mn^{2+} in CdSe QDs was shown to be feasible with a fourth method, the so-called cluster method. Here, well-selected organometallic cation clusters are used as precursor in a method that resembles the hot injection method (similar coordinating ligands, growth at elevated temperatures) but involves a controlled rise to the reaction temperature.[34] With this method, the successful incorporation of Co^{2+} and Mn^{2+} in CdSe QDs was demonstrated, yielding paramagnetic and luminescent QDs.[35]

The potential of QDs doped with paramagnetic ions as multimodal probes (magnetic and luminescent) in imaging has been realized only recently. Most work in the past was aimed at the use of doped QDs in light-emitting devices and exploiting the magnetic properties in the field of spintronics with a focus on ferromagnetism in dilute magnetic semiconductor (DMS) nanoparticles.[28] In a paper by Santra et al., the use of CdS:Mn/ZnS QDs (Type IIa) for bimodal imaging was demonstrated.[36] Using the inverse micelle method, 3.1-nm particles were synthesized and coated with a thin silica layer, which was further modified with APS to include amine surface groups for bioconjugation. The QDs showed a bright yellow Mn^{2+} emission and exhibited a clear magnetic response (Figure 4(a)). The capability for *in vivo* imaging was demonstrated by conjugating the QDs with a HIV-1 trans-activator of transcription (TAT) peptide. The HIV-1 TAT-peptide-conjugated QDs were administered in the right common carotid artery that supplies blood to the right part of the rat's brain. The results in Figure 4(b) and (c) show

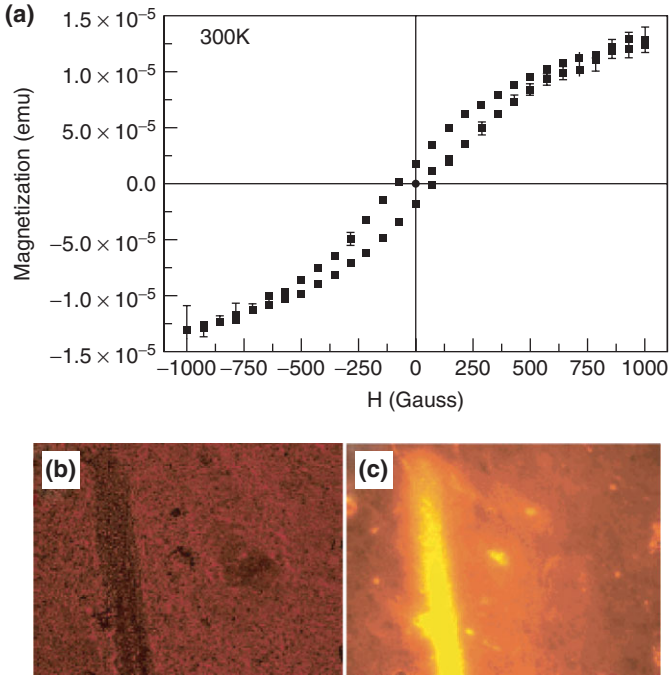

FIGURE 4 | (a) Magnetization curve for CdS:Mn/ZnS quantum dots (QDs). (b) Transmission and (c) fluorescence microscopy images of a cross-section of the brain showing branches of the right middle cerebral artery after labeling with HIV-1 TAT-conjugated CdS:Mn/ZnS QDs. (Reprinted, with permission, from Ref. 36. Copyright 2005 American Chemical Society.)

the labeling of right middle cerebral artery, and the authors conclude that these labels can cross the blood–brain barrier, suggesting a potential for this type of label for imaging of, for example, brain tumors. Although magnetization curves of this particle were obtained, this feature was not further exploited by MRI.

Bimodal imaging with CdSe/$Zn_{1-x}Mn_xS$ nanoparticles (Type IIb) was demonstrated by the group of Louie.[37] In this core/shell particle, the highly luminescent (undoped) CdSe core was overgrown with a ZnS shell that was doped with Mn^{2+} to introduce the paramagnetic functionality (Figure 5(a)). The fluorescence from this bimodal particle originated from the CdSe core and had a QE of over 20%. The paramagnetic Mn^{2+} ions are situated in the outer shell, which facilitates a good interaction with water, thereby serving as an efficient MRI contrast agent. The nanoparticles (~5 nm) were made water soluble by a coating of octyl-amine-modified poly(acrylic)acid (see Figure 5(a)). The influence of the number of paramagnetic Mn^{2+} ions in the shell on the T_1 relaxation times was analyzed and resulted in r_1 values ranging form 10 upto 18 mM^{-1} s^{-1}. Finally, the suitability as a bimodal contrast agent was demonstrated by incubating macrophages with these nanoparticles. The uptake of the CdSe/$Zn_{1-x}Mn_xS$ core/shell particles was verified by both confocal fluorescence microscopy (Figure 5(b)) and MRI (Figure 5(c)).

A serious drawback for Cd-containing QDs is the toxicity of Cd. There is a strong effort to develop Cd-free QDs for biological imaging applications. In a recent publication, Kauzlarich et al. reported on silicon nanoparticles doped with Mn^{2+}.[38] The doping with Mn^{2+} caused a red shift of the QD emission from 430 to 520 nm, while retaining a high quantum yield (up to 16%). On the basis of EPR and transient absorption spectra, it was concluded that the Mn^{2+} is incorporated in the nanocrystal and is strongly coupled to the Si surface. These results are an encouraging step toward the development of doped Si QDs as multimodal labels for imaging.

In the future one may envisage that doped QDs that are luminescent and ferromagnetic will be employed as a combined fluorescence and MRI probe. Work on, for example, ZnO:Mn^{2+} and ZnO:Co^{2+} has demonstrated ferromagnetic ordering in these nanocrystals, induced by oxygen defects.[39] The ferromagnetic properties may be exploited to develop contrast agents for T_2-weighted MRI. Altogether, doping QDs with paramagnetic ions has shown remarkable changes in the optical properties of such QDs. Importantly, the most recent developments also demonstrate their applicability for MRI purposes.

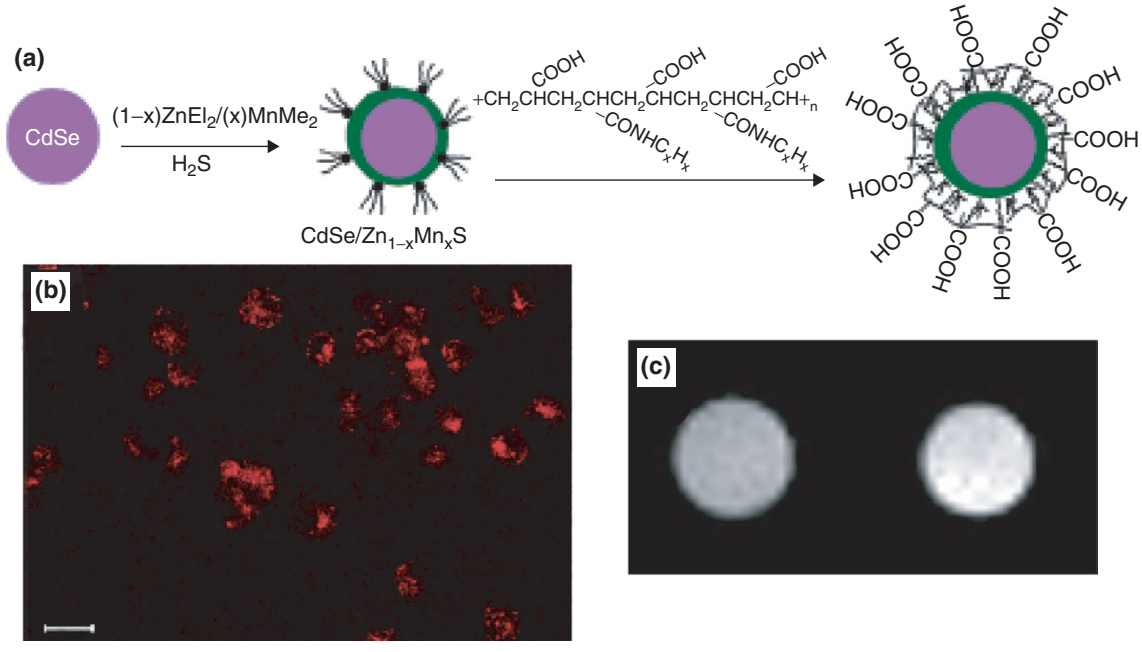

FIGURE 5 | (a) Synthetic route for generation of polymer-coated, water-soluble core/shell CdSe/$Zn_{1-x}Mn_xS$ quantum dots (QDs), and (b) their uptake by macrophages shown by confocal fluorescence microscopy (scale bar 20 μm). (c) T_1-weighted MRI on the lysates of cells that were incubated with the doped QDs (right) shows a stronger contrast compared to cells that were not incubated (left). (Reprinted, with permission, from Ref. 37. Copyright 2007 American Chemical Society.)

Composite Particles Containing Magnetic and Semiconductor Nanoparticles (Type III)

Another approach to add magnetic functionalities to QDs is by using a carrier material to create a composite particle in which both magnetic and semiconductor nanocrystals can be integrated. The different types of NPs can be either incorporated *in* the carrier material (Figure 1, Type IIIa), *attached to* the outside of the carrier material, or a combination of both, in which, for example, the QD is incorporated *in* the carrier particle and the MNPs are *attached to* the outside of the carrier particle (Figure 1, Type IIIb). Both silica and polymer matrices can be used as a carrier material as will be discussed below, resulting in a construct that is generally larger than particles of Type I or Type II. The first part of this section will focus on composite particles using silica as a carrier material, and the second part will discuss the use of polymer capsules as carrier material.

Composite particles that resemble Type IIIa particles in Figure 1 were synthesized by Yi et al., who inserted both Fe_2O_3 MNPs and CdSe/Zns QDs in silica spheres of ~50 nm (Figure 6(a), left and right panel).[40] The composite particles were synthesized by adding separately prepared MNPs (12 nm) and QDs (3.5 nm) to a standard microemulsion system.[41,42] This yielded monodisperse silica particles with multiple MNPs and QDs incorporated. Incorporation in silica reduced the QE of the CdSe/ZnS QDs from 15% to 5%, and the QDs exhibited an emission peak at 554 nm. The reason for the reduction of the QE was not mentioned, but it may be due to an interaction with the magnetic particles (as described earlier), or a direct effect of the incorporation of QDs in a silica matrix using the microemulsion method.[43] Although not shown by the authors, this approach should be applicable to QDs of different sizes and therefore allow variation in the emission wavelength. The superparamagnetic properties of the MNPs within the silica spheres were confirmed by the blocking temperature (T_b) of 165 K, and the magnetization at saturation did not change as a result of the addition of the QDs. A similar composite particle of iron oxide MNPs and QDs was reported by Kim and coworkers, by incorporating both types of nanocrystals in larger (150 nm) mesoporous silica spheres.[44]

An approach to reduce interactions between the MNPs and the QDs is to increase the interparticle distance. Such a composite particle is schematically depicted as Type IIIb in Figure 1, of which a practically realized example is shown in Figure 6(b). In this case, Salgueiriño-Maceira et al. used a Stöber approach[47] to incorporate iron oxide (a mixture of Fe_3O_4 and γ-Fe_2O_3) MNPs in silica spheres.[45] The MNPs were 30 nm in diameter and surrounded by a silica shell of 70 nm. Subsequently, the silica spheres were coated by positively charged polymers, enabling the deposition of negatively charged CdTe QDs by a well-established layer-by-layer (LbL) deposition technique (insert in Figure 6(b)). Finally, the silica particles with a magnetic core and fluorescent shell were coated with a second silica shell of 20 nm, resulting in final composite particles with a diameter of 220 nm. Both green- and red-emitting QDs could be attached to the silica surface. Although it was not possible to measure the QE of the CdTe QDs because of light scattering of the large silica particles, the authors state that the relatively long distance between the MNPs and the QDs circumvented quenching of the QD emission. The magnetic properties of the composite particles were determined using a superconducting quantum interference device (SQUID), from which a blocking

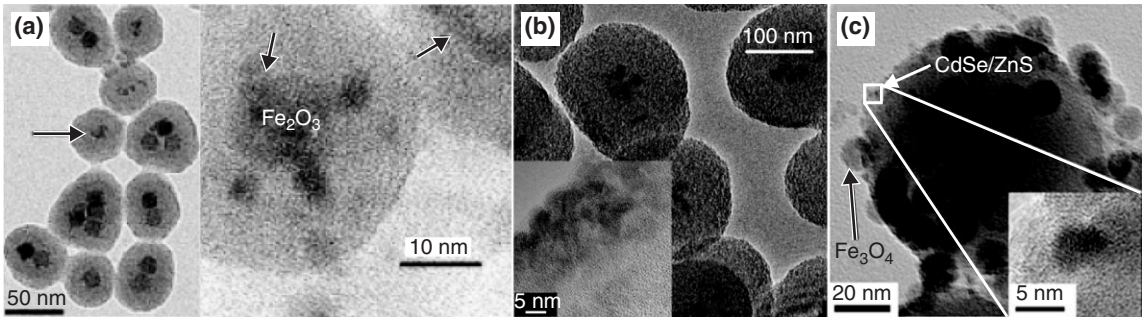

FIGURE 6 | (a) TEM image of composite silica particles with Fe_2O_3 MNPs and CdSe quantum dots (QDs) incorporated (right panel shows a magnified image), reprinted with permission from Ref. 40. Copyright (2005) American Chemical Society. (b) TEM image of multiple iron oxide MNPs incorporated in 170-nm silica spheres. Enlarged image of the silica surface (insert) shows the presence of small CdTe QDs. Reproduced with permission from Ref. 45. Copyright Wiley-VCH Verlag GmbH & Co.KGaA. (c) TEM image of CdSe/ZnS QDs (4.5 nm) and Fe_3O_4 MNPs (14 nm) both attached to the surface of 100-nm silica particles. Insert shows a magnified image of the silica surface with a QD attached. (Reprinted, with permission, from Ref. 46. Copyright 2006 Wiley-VCH Verlag GmbH & Co.KGaA.)

temperature (T_b) of 150 K, a coercivity of 175 Oe (at 5 K), and saturation magnetization of 1.34 emu/g were obtained.

The final example of silica as carrier material for MNPs and QDs that we will discuss here was reported by the group of Hyeon. In this case, both types of nanocrystals were attached to the outside of 100-nm silica spheres (Figure 6(c)).[46] The silica spheres were synthesized by a Stöber approach,[47] and the surface was functionalized by amine groups using APS. Subsequently, 2-bromo-2-methylpropane acid (BMPA)-functionalized Fe_3O_4 particles were covalently attached to the silica surface by a nucleophilic substitution reaction between the terminal Br groups of the ligands and the amine groups of the silica spheres. In addition, CdSe/ZnS QDs could be attached to the silica surface by direct binding to the amine groups of the silica surface (insert in Figure 6(c)). The final composite particles were 100 nm in size and heavily loaded with both Fe_3O_4 MNPs (14 nm) and CdSe/ZnS QDs (4.5 nm). It was shown that both green- and red-emitting QDs could be attached to the silica surface. Magnetic characterization revealed no hysteresis of the MNPs on silica spheres at 300 K, confirming that the iron oxide particles were superparamagnetic. A subtle example of a possible application of such particles was shown by confocal microscopy of a mixture of green QDs attached to silica *without* MNPs attached and red-emitting QDs attached to silica spheres *with* MNPs attached. After removal of the latter particles by a magnet, the dispersion showed only green luminescence, illustrating how these particles could be used for cell separation.[48–50] A similar separation experiment was conducted by Sathe and coworkers, who used mesoporous silica particles (3–5 μm with 30-nm pores) embedded with QDs and MNPs (Type IIIa).[51]

In addition to silica, polymer microcapsules can be used as a carrier material to combine magnetic NPs and QDs. This approach was first reported by Gaponik and coworkers, who incorporated 8-nm Fe_3O_4 MNPs and 3–6-nm CdTe QDs (QE of 15–30%) in hollow polymer microcapsules (5.6 μm) consisting of two oppositely charged polyelectrolytes (PEs).[52] This was achieved by the penetration of negatively charged NPs through the 10-nm pores of the microcapsules, resulting in a composite particle of Type IIIa. The fluorescent and magnetic properties of these microcapsules were elegantly confirmed by aligning the spheres in a magnetic field and probing the fluorescence of the particles with a confocal microscope (Figure 7(a)).

Another method to synthesize polymer nanocomposite particles of Type IIIa was reported by Xie et al., using styrene/acrylamide copolymer nanospheres of which the size could be varied between 50 and 500 nm.[53] Hydrophobic γ-Fe_2O_3 (5–20 nm) and CdSe/ZnS (3–6 nm) were incorporated in these polymer nanospheres (Figure 7(b)) in a ratio that can be easily adjusted, for example, to prevent reabsorption of the QD emission by the MNPs. Pegylated molecules with a folic acid group were attached to the surface of the nanospheres to specifically target them to tumor cells, which overexpress a glycoprotein that is a receptor for folic acid. The authors showed that after 3–6 h of incubation, the cancer cells could be efficiently separated from a suspension by a magnet, after which the separated cells could be investigated by fluorescence microscopy. The separated cells exhibited a bright luminescence, and control experiments showed that there was no aspecific association of the particle with the tumor cells.

A final example of polymers as a carrier material for MNPs and QDs was reported by Hong and coworkers, who encapsulated Fe_3O_4 MNPs of 8.5 nm by alternating layers of positively and negatively charged PEs using an LbL technique[54] (Figure 7(c)). Negatively charged CdTe QDs could be readily integrated between the positively charged PEs. The advantage of this system is that the distance between the QDs and MNP can be tuned by inserting a variable number of PE layers in between two layers of particles. This was exploited to study the influence of the distance between the QDs and MNPs on the emission intensity. It was found that the QD fluorescence strongly increases with increasing interparticle distance. The authors explain this finding by a combination of two effects: the first effect is a distance-dependent quenching mechanism of the fluorescence by the MNPs, and the second is due to the increase of surface area at larger distances resulting in an increase in the amount of CdTe QDs that can attach. An important advantage of this LbL method is that multiple layers of QDs can be integrated, and the type of particles is not limited to QDs only. For example, negatively charged metal or MNPs can also be integrated, and bioactive materials such as enzymes or pharmaceutical agents may be incorporated or attached as well.[55,56]

The above-mentioned examples show that composite particles using silica or polymers as carrier materials can be synthesized in many flavors. Clear advantages of this versatile approach are, for example, the high payload of MNPs or QDs that can be integrated, the tunability of the ratio between the NPs,

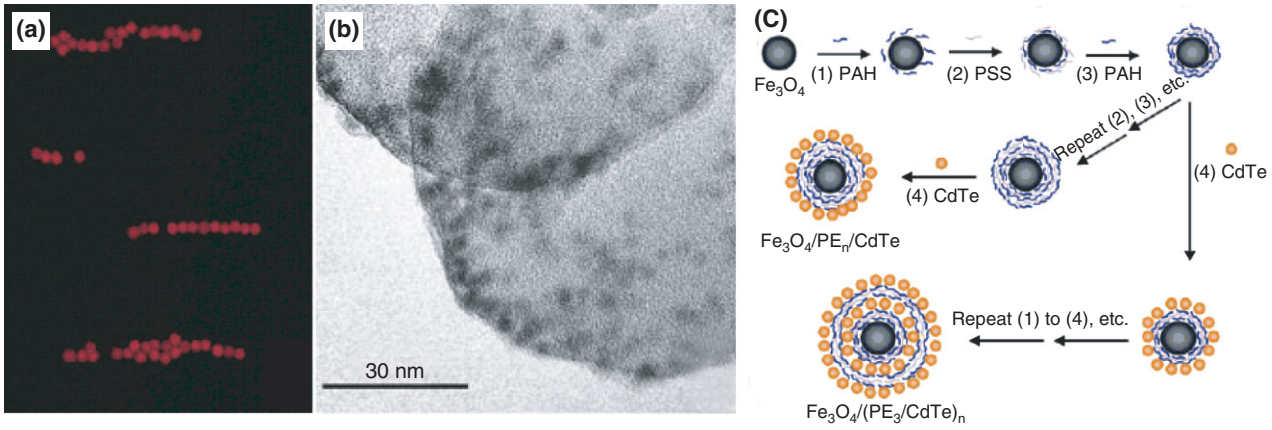

FIGURE 7 | (a) Confocal microscope image of 5.6–μm polymer microcapsules containing red-emitting CdTe quantum dots (QDs) and Fe_3O_4 MNPs, aligned by an external magnetic field. Reprinted with permission from Ref. 52. Copyright (2004) American Chemical Society. (b) TEM image of a ~100−nm copolymer nanosphere embedded with both CdSe/ZnS QDs and Fe_2O_3 MNPs. Reproduced with permission from Ref. 53. Copyright Wiley-VCH Verlag GmbH & Co. KGaA. (c) Schematic representation of the synthesis of Fe_3O_4 MNPs encapsulated by both positively (PAH) and negatively (PSS) charged polyelectrolytes (PEs). After deposition of the PEs (steps 1–3), negatively charged QDs were attached (step 4). Multilayers of QDs could be embedded by repeating steps 1 to 4. (Reprinted, with permission, from Ref. 54. Copyright 2004 American Chemical Society.)

and the control over the distance between the MNPs and QDs. Furthermore, the emission wavelength of the QDs can be easily varied by integrating (a combination of) different QDs, allowing for multiplexing or 'barcoding'.[57] The surface chemistry of silica particles and polymer microcapsules is well developed, facilitating the biofunctionalization of these carriers. A distinct and inherent feature of composing nanoparticles of a carrier material and nanocrystals is their relatively large size (>50 nm). This likely poses a limit on their applicability to target extravascularly, but enhances their suitability for targeting receptors at the endothelial cells of blood vessels. In addition, renal clearance of these larger particles does not occur, which probably increases their blood circulation half-life. This may be considered an advantage in some cases, but might limit clinical applications.

QDs with a paramagnetic coating of Gd-chelates (Type IV)

The fourth and final category of particles that will be discussed here are defined as QDs coated by organic complexes (chelates) containing paramagnetic ions, schematically shown as Type IV in Figure 1. The lanthanide ion Gd^{3+} is the most widely used paramagnetic ion for MRI contrast agents, because it has a high magnetic moment and a symmetric electronic ground state. To decrease toxicity and enhance stability, the Gd^{3+} ions are complexated in organic chelates that coordinate to the paramagnetic ions through an ionic interaction. One of the most widely used MRI contrast agents for experimental and clinical use is Gd-DTPA (diethylenetriaminepentaacidic acid), but there is a wide variety of other compounds being studied to optimize the molar relaxivity as well as to explore the range of useful biomedical applications.[58] In order to introduce fluorescent properties to the paramagnetic chelates, organic dye molecules have been attached to the complexes both covalently[59,60] and noncovalently.[61] Another strategy to achieve this bimodality (MRI and fluorescence imaging) is by attaching the paramagnetic chelates to QDs. This can also be achieved by either covalent or noncovalent attachment to the QD, of which a few examples will be discussed below.

The first example of combining paramagnetic chelates with QDs was reported by Mulder et al., who used a lipidic micelle surrounding a QD to (noncovalently) integrate Gd-DTPA complexes.[19] It had been reported earlier that hydrophobic QDs could be rendered bioapplicable by encapsulating QDs in the hydrophobic interior of lipidic micelles.[3] Mulder et al. adapted this method to coat CdSe/ZnS QDs by a combination of pegylated (PEG-DSPE) and paramagnetic (Gd-DTPA-BSA) lipids (Figure 8(a)). The paramagnetic lipids consisted of two hydrophobic stearylamide chains (BSA) attached to a Gd-DTPA complex. The resulting paramagnetic and pegylated QDs of Type IVa exhibited a bright and narrow emission band around 560 nm, and (although not reported) the approach allows one to choose any type (size) of hydrophobic QD to tune the emission color. The ionic relaxivity r_1 of Gd-DTPA-BSA was

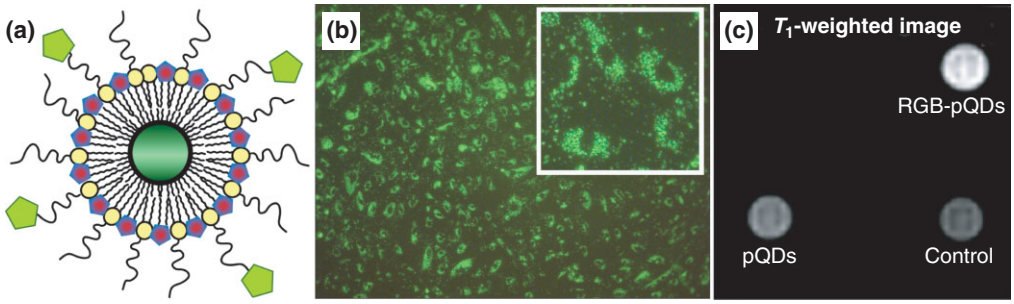

FIGURE 8 | (a) Schematic drawing of a quantum dot (QD) (green) encapsulated in pegylated (red) and paramagnetic (yellow) lipids. A small fraction of the pegylated lipids was functionalized by an arginine-glycine-aspartic acid (RGD) peptide, which enables targeting to a cell surface receptor (green). (b) Fluorescence microscopy image of human umbilical vein endothelial cells (HUVEC) incubated with RGD-conjugated paramagnetic QDs. (c) T_1-weighted magnetic resonance imaging (MRI) images of cell pellets incubated with RGD-conjugated (upper right) or nonconjugated (bottom left) QDs, or not incubated at all (control). (Reprinted, with permission, from Ref. 19. Copyright 2006 American Chemical Society.)

determined to be 12.4 mM^{-1} s^{-1}, which is a factor of 3 higher than that of free Gd-DTPA. This is due to the lower tumbling rate of the Gd-DTPA-BSA complex (because it is incorporated in the micelle) as compared to free Gd-DTPA.[58,62] The ionic relaxivity r_2 was 18 mM^{-1} s^{-1}, and because the r_2/r_1 ratio is 1.5, the particles are suitable for T_1-weighted imaging.

To target the paramagnetic QDs, a fraction of the pegylated lipids was distally equipped with a maleimide group to which a biofunctional molecule (in this case cyclic RGD) could be covalently linked. Cyclic RGD specifically binds to the $\alpha v\beta_3$−integrin receptor that is overexpressed at the surface of human umbilical vein endothelial cells (HUVEC). When these cells were incubated with the RGD-conjugated paramagnetic QDs, a high cellular uptake was observed at a perinuclear location (Figure 8(b) and insert). The bimodality and specificity of the paramagnetic QDs were confirmed by MRI on cell pellets, which were incubated with RGD-conjugated and nonconjugated particles. Compared to the control cell pellet (no particles incubated, $T_1 = 1966$ ms), cells incubated with the nonconjugated particles showed a slightly stronger signal on T_1-weighted MRI scans ($T_1 = 1673$ ms), which demonstrated that there was a low degree of aspecific uptake by the cells (Figure 8(c)). However, the cell pellet that was incubated with RGD-conjugated particle exhibited a much brighter MRI signal ($T_1 = 1123$) as compared to the other pellets, confirming the target-specific uptake of the lipid-coated QDs and their favorable MRI contrast properties. In another study, the paramagnetic and pegylated QDs were conjugated with annexin A5 protein molecules for targeting apoptotic cells.[63] Again, fluorescence imaging and MRI confirmed the specificity and bimodal character of these particles.

The paramagnetic QD-based contrast agent discussed above was used to conduct molecular imaging of tumor angiogenesis using intravital microscopy, MRI, and fluorescence imaging. To this aim, tumor-bearing mice were intravenously injected with the contrast agent and were studied with the aforementioned imaging techniques *in vivo*. Intravital microscopy was used for the real-time monitoring of the fate of injected QDs at cellular level. In Figure 9(a), a fluorescence image of blood vessels of a tumor is depicted 30 min after the injection of contrast agent. High-resolution T_1-weighted MRI was performed before and after applying the agent. Figure 9(b) displays a color-coded image generated from the MRI data before and 45 min after the contrast agent injection. The MRI voxels that showed significant signal enhancement following RGD-conjugated QD-micelle injection were mainly found at the tumor periphery, which corresponds with the regions of the tumor with highest angiogenic activity. Lastly, fluorescence imaging of nude mice with renal carcinoma tumors was done upon injection of the contrast agent. Strong fluorescent signal originating from the tumor was observed (Figure 9(c)).

An alternative way to obtain QDs coated with a paramagnetic coating of Gd-chelates was reported by Prinzen et al.[65] Instead of using a lipidic coating around the QD, the authors used biotinylated Gd-DTPA and biotinylated annexin A5 proteins, which were both coupled to streptavidin-coated QDs. In addition, a novel biotinylated dendrimer-like chelate (Gd-wedge) was developed containing eight Gd-DTPA complexes per wedge, with the aim of enhancing the detection sensitivity in MRI. In this study, both green- and red-emitting QDs were used, and the ionic relaxivities r_1 of the Gd-DTPA and Gd-wedges were determined to be 17.5 and 15.6 mM^{-1} s^{-1}, respectively, which

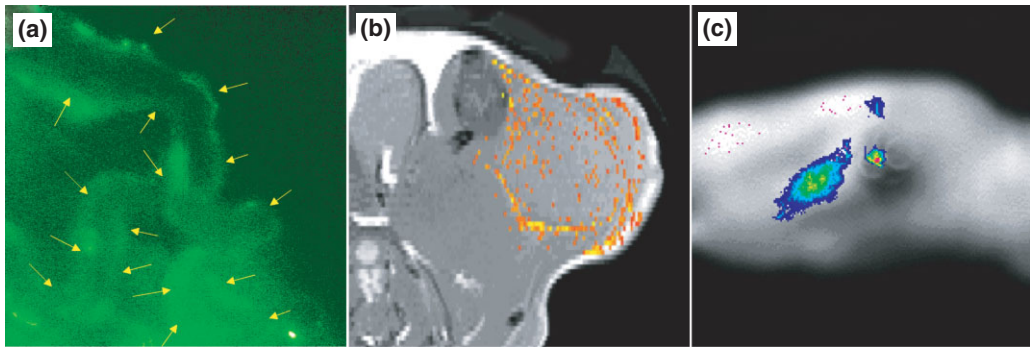

FIGURE 9 | Multimodality imaging of tumor angiogenesis in mice. (a) Intravital microscopy of tumor blood vessels, (b) magnetic resonance imaging (MRI) of regions with high angiogenic activity in a subcutaneously growing tumor, and (c) fluorescence imaging of tumor angiogenesis feasible after intravenous administration of paramagnetic quantum dot (QD) micelles (as described in Ref. 19). Taken from Ref. 64.

are high compared to free Gd-DTPA as mentioned before. Using fluorescence imaging and MRI, strong labeling of apoptotic Jurkat cells by the QD-Gd-wedge particles was demonstrated *in vitro*, whereas aspecific binding was low. Furthermore, target-specific labeling was performed on an excised murine carotid artery that was mechanically injured, resulting in an overexpression of PS (phosphatidylserine, binds to annexin A5). The damaged artery showed a high uptake of the green-emitting, annexin-5-conjugated QD-Gd-wedge particles, as was demonstrated by two-photon laser scanning microscopy (Figure 10(a)). The target specificity was confirmed by the fact that an undamaged control artery hardly showed any labeling. *Ex vivo* T_1-weighted MRI showed a brighter signal for the damaged artery as compared to the control artery, confirming the utility of the bimodal nanoparticles (Figure 10(b)).

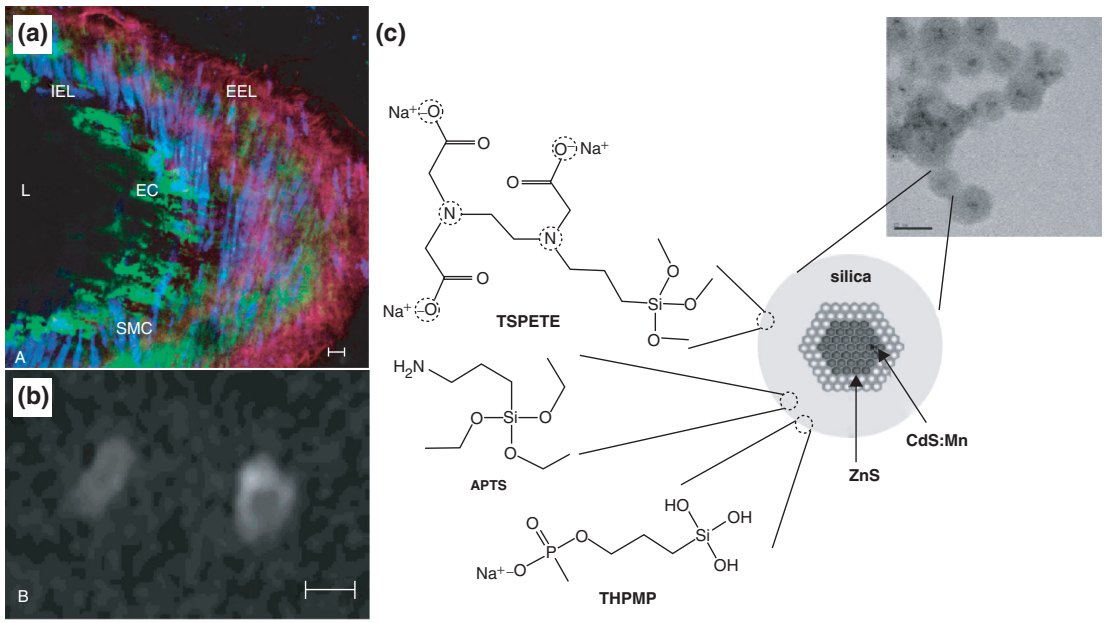

FIGURE 10 | (a) Two-photon laser scanning microscopy image of a damaged murine carotid artery (*ex vivo*), showing high uptake of green-emitting, annexin A5-conjugated QDs with a Gd-wedge coating in ECs and SMCs. EC, endothelial cells; SMC, smooth muscle cells; L, lumen; IEL, internal elastic lamina; EEL, external elastic lamina. Red: eosin, labeling elastin laminae; blue: syto41, labeling cell nuclei. (b) The same damaged artery shows a brighter contrast in an MR image (right) compared to an undamaged control artery (left). (a) and (b) are reprinted with permission from Ref. 65. Copyright (2007) American Chemical Society. (c) Design of a silica-coated QD with negatively charged (THPMP), positively charged (APTS), and paramagnetic complexes (TSPETE) covalently bound to the silica surface. The dotted circles in the TSPETE complex represent the five coordination sites for Gd ions. Insert shows a TEM image of the particles. (Reprinted, with permission, from Ref. 66. Copyright 2006 Wiley-VCH Verlag GmbH & Co. KGaA.)

The overall relaxivity (and hence the detection threshold in MRI) of particles coated by paramagnetic chelates will depend on the number of these complexes that can be attached per QD. It may therefore be interesting to increase the surface area of the QDs by first coating the QDs with another material before applying the paramagnetic coating (Type IVb). One example of such a design was reported by the group of Holloway, who reported the synthesis of 3-nm CdS:Mn/ZnS QDs in a reverse micelle, to which silica precursors could be directly added for the growth of a 7-nm silica shell[66] (insert Figure 10(c)). The silica shell was terminated by both positively charged amine groups and negatively charged phosphonate groups to enhance the water solubility of the particles. To introduce paramagnetic properties, TSPETE (a chelate with a silane coupling agent that can capture five Gd^{3+} ions) was covalently attached to the silica surface (Figure 10(c)). The resulting particles exhibited a Mn-related yellow emission with a QE of 28%, and were highly photostable. The values for the ionic relaxivity r_1 and r_2 were determined to be 20.5 and 151 mM^{-1} s^{-1}, respectively, which indicates that these particles are most suitable for T_2-weighted imaging.

A similar architecture of Type IVb was reported by Gerion and coworkers, by applying a thin (2–3 nm) silica shell around CdSe/Zns QDs.[67] Paramagnetic properties were introduced by gadolinium-1,4,7,10-tetraazacyclododecane-*N*,*N*′,*N*″,*N*‴-tetraacetic acid (Gd-DOTA) chelates with a maleimide group, which allowed covalent linkage to the thiol-terminated silica surface. According to the authors, the advantages of their method are the simplicity of the synthesis procedure, the flexibility in composition, and the high ionic relaxivity r_1 of 23 mM^{-1} s^{-1}. The latter was ascribed to the relatively low tumbling rate of the fixed Gd-chelates, as discussed above.

The paramagnetic functionality of the Type IV particles discussed in this section is intrinsically localized at the outer surface of the QD, because the Gd-chelates require a direct and fast interaction with water molecules to obtain a higher r_1 value. As a result, more effort has been put in the surface chemistry of these particles, including the integration of biocompatible and biofunctional groups. This explains the more advanced stage of development of these Type IV particles for biomedical applications as compared to the other designs discussed in this review. By directly applying the chelate coating around the QD (Type IVa), the final particle size is small (< 10 nm), which may be favorable for reaching a broad range of targets that are of biomedical interest. On the other hand, the size of the particles can be increased by inserting an intermediate layer (e.g., a silica coating) between the QD and the paramagnetic coating, thereby increasing the surface area and the payload of chelates that can adhere to the surface (Type IVb). Although the magnetic moment of the Type IV particles is probably too low for applications like cell separation, they are well suited for T_1-weighted MRI. Further *in vivo* testing is needed to establish which of the preparation strategies discussed above is the most suitable for target-specific bimodal imaging applications.

The biochemical safety profile of Gd-chelates described above has been extensively studied.[68] These studies have led to the conclusion that Gd-based MRI contrast agents are generally very safe to use and very well tolerated. Recently, an association has been suggested between the use of Gd agents and the incidence of nephrogenic systemic fibrosis (NSF) in dialysis patients or patients with end-stage renal failure, in whom the rate of agent clearance is strongly impaired. For these reasons, the safety profiles of novel Gd agents, such as the ones discussed in this review, should be carefully studied when considered for translational purposes.

SUMMARY AND OUTLOOK

In this review we have discussed four different architectures of magnetic QDs that have been reported to date. The core/shell and heterostructures (Type I) have the main advantage of being relatively small (<10 nm), but the QE and wavelength tunability of the particles is still limited. On the other hand, this approach has only recently been developed, so significant improvement may be expected in the future. The doped QDs (Type II) can even be made smaller (<5 nm), which may enhance the clinical applications as will be discussed below. In view of the toxicity of the cadmium-based QDs, a promising alternative design of doped QDs is offered by the use on Mn-doped silicon particles.[38] The composite particles that consist of a carrier material in which MNPs and QDs are integrated (Type III) are generally fairly large (>50 nm). However, this approach is clearly the most versatile because the type of QD or MNP can be easily varied as well as the ratio between the two, and high payloads of contrast agent can be achieved. The last category discussed in this review is defined as QDs with a paramagnetic coating of Gd-chelates (Type IV). Besides the small size of the particles (>10 nm), the advantage of this approach is that there is no interaction between the QD and magnetic coating, thereby allowing a high QE. On the other hand, the paramagnetic payload is limited for the smallest particles.

As is evident from comparing the different strategies discussed in this review, the general trade-off is between particles with a small size but limited payload on one hand, and larger particles with a higher and more flexible payload of contrast agents on the other. Depending on the goals of the bioimaging study, different properties (size, payload, composition) of the contrast agents are required. For example, the use of larger particles with high contrast sensitivity is favourable for vascular targeting, whereas extravascular targeting requires small contrast agents for penetration to deeper-lying tissues. Another consideration is the utilization of positive (i.e., T_1-weighted MRI using Gd-chelates) or negative (i.e., T_2-weighted MRI using MNPs) contrast, which will depend on the sensitivity that is desired and the tissue that is aimed for. Finally, the size of the particles determines the mechanism and speed at which they are cleared from the blood circulation. It was recently reported that only QDs smaller than 5.5 nm were rapidly eliminated from the blood circulation of mice by renal excretion.[69] On one hand this fast urinary clearance from the body is favourable in view of the toxicity of the cadmium-containing QDs; on the other, longer circulation times are desired in case of targeted studies, to allow efficient binding of the contrast agents to the specific receptors. Because of the large variety in demands for the different bioimaging applications, it is foreseen that each of the strategies discussed here will be further explored.

It is beyond the scope of this review to evaluate which type or design of particle is the most advantageous or promising for bioapplications. For that purpose, the comparison should not be restricted to the physicochemical characterization of the quantum efficiency, relaxivity, contrast payload, or size of the nanoparticles. Whether a bimodal contrast agent will be successful truly depends on the performance of the particles *in vivo*, which still has to be tested for most of the particles discussed here. Important features for successful *in vivo* application of contrast agents are, for example, the circulation half-time of the particles and the mechanisms by which they are cleared (kidneys, liver, or elsewhere). Furthermore, the target specificity and imaging sensitivity of the particles *in vivo* may significantly differ from their characteristics *in vitro*.

Last but not least, the toxicity of contrast agents based on (cadmium containing) QDs is an important issue that has to be resolved. The toxic effects of nanoparticles, and specifically that of QDs, depend on a wide range of properties, such as their size, concentration, and their surface coating. Heavy metal ions (e.g., Cd^{2+}) were, for example, observed to dissociate in time from CdSe QDs and to cause cell death, whereas CdSe/ZnS QDs were found to be nontoxic to hepatocytes during an incubation period of 2 weeks.[70] Aside from the chemical content of the nanoparticle surface, particle cytotoxicity was also found to depend on surface charge and stability against particle aggregation.[71] Neutral surfaces and surfaces coated with stabilizing agents may prevent particle aggregation and increase cell viability rates.[72] It must be noted that the efficacy of these coating strategies in diminishing cytotoxic effects must be evaluated for every newly developed coating. This also applies to the *in vivo* toxic effects of QDs,[73] which are still largely unknown.[74]

REFERENCES

1. Chan WCW, Nie S. Quantum dot bioconjugates for ultrasensitive nonisotopic detection. *Science* 1998, 281(5385):2016–2018.
2. Bruchez M Jr, Moronne M, Gin P, Weiss S, Alivisatos AP. Semiconductor nanocrystals as fluorescent biological labels. *Science* 1998, 281(5385):2013–2016.
3. Dubertret B, Skourides P, Norris DJ, Noireaux V, Brivanlou AH, et al. In vivo imaging of quantum dots encapsulated in phospholipid micelles. *Science* 2002, 298(5599):1759–1762.
4. Gao XH, Cui YY, Levenson RM, Chung LWK, Nie SM. In vivo cancer targeting and imaging with semiconductor quantum dots. *Nat Biotechnol* 2004, 22(8):969–976.
5. Stroh M, Zimmer JP, Duda DG, Levchenko TS, Cohen KS, et al. Quantum dots spectrally distinguish multiple species within the tumor milieu in vivo. *Nat Med* 2005, 11(6):678–682.
6. Medintz IL, Clapp AR, Mattoussi H, Goldman ER, Fisher B, et al. Self-assembled nanoscale biosensors based on quantum dot FRET donors. *Nat Med* 2003, 2(9):630–638.
7. So M-K, Xu C, Loening AM, Gambhir SS, Rao J. Self-illuminating quantum dot conjugates for in vivo imaging. *Nat Biotechnol* 2006, 24(3):339–343.
8. Schipper ML, Cheng Z, Lee S-W, Bentolila LA, Iyer G, et al. MicroPET-based biodistribution of quantum dots in living mice. *J Nucl Med* 2007, 48(9):1511–1518.

9. Daneshvar H, Nelms J, Muhammad O, Jackson H, Tkach J, et al. Imaging characteristics of zinc sulfide shell, cadmium telluride core quantum dots. *Nanomedicine* 2008, 3(1):21–29.
10. Strijkers GJ, Mulder WJM, van Tilborg GAF, Nicolay K. MRI contrast agents: current status and future perspectives. *Anticancer Agents Med Chem* 2007, 7(3):291–305.
11. Caravan P, Ellison JJ, McMurry TJ, Lauffer RB. Gadolinium(III) chelates as MRI contrast agents: structure, dynamics, and applications. *Chem Rev* 1999, 99(9):2293–2352.
12. Bulte JWM, Kraitchman DL. Iron oxide MR contrast agents for molecular and cellular imaging. *NMR Biomed* 2004, 17(7):484–499.
13. Gupta AK, Naregalkar RR, Vaidya VD, Gupta M. Recent advances on surface engineering of magnetic iron oxide nanoparticles and their biomedical applications. *Nanomedicine* 2007, 2(1):23–39.
14. Kwon KW, Shim M. γ-Fe2O3/II-VI sulfide nanocrystal heterojunctions. *J Am Chem Soc* 2005, 127(29):10269–10275.
15. Gao JH, Zhang B, Gao Y, Pan Y, Zhang XX, et al. Fluorescent magnetic nanocrystals by sequential addition of reagents in a one-pot reaction: a simple preparation for multifunctional nanostructures. *J Am Chem Soc* 2007, 129(39):11928–11935.
16. Gu H, Zheng R, Zhang X, Xu B. Facile one-pot synthesis of bifunctional heterodimers of nanoparticles: a conjugate of quantum dot and magnetic nanoparticles. *J Am Chem Soc* 2004, 126(18):5664–5665.
17. Kim H, Achermann M, Balet LP, Hollingsworth JA, Klimov VI. Synthesis and characterization of Co/CdSe core/shell nanocomposites: Bifunctional magnetic-optical nanocrystals. *J Am Chem Soc* 2005, 127(2):544–546.
18. Selvan ST, Patra PK, Ang CY, Ying JY. Synthesis of silica-coated semiconductor and magnetic quantum dots and their use in the imaging of live cells. *Angew Chem Int Ed Engl* 2007, 46(14):2448–2452.
19. Mulder WJM, Koole R, Brandwijk RJ, Storm G, Chin PTK, et al. Quantum dots with a paramagnetic coating as a bimodal molecular imaging probe. *Nano Lett* 2006, 6(1):1–6.
20. Veiseh O, Sun C, Gunn J, Kohler N, Gabikian P, et al. Optical and MRI multifunctional nanoprobe for targeting gliomas. *Nano Lett* 2005, 5(6):1003–1008.
21. Dubois F, Mahler B, Dubertret B, Doris E, Mioskowski C. A versatile strategy for quantum dot ligand exchange. *J Am Chem Soc* 2007, 129(3):482–483.
22. Michalet X, Pinaud FF, Bentolila LA, Tsay JM, Doose S, et al. Quantum dots for live cells, in vivo imaging, and diagnostics. *Science* 2005, 307(5709):538–544.
23. Gerion D, Pinaud F, Williams SC, Parak WJ, Zanchet D, et al. Synthesis and properties of biocompatible water-soluble silica-coated CdSe/ZnS semiconductor quantum dots. *J Phys Chem B* 2001, 105(37):8861–8871.
24. Klasens HA. On the nature of fluorescent centers and traps in zinc sulfide. *J Electrochem Soc* 1953, 100(2):72–80.
25. Bhargava RN, Gallagher D, Hong X, Nurmikko A. Optical properties of manganese-doped nanocrystals of ZnS. *Phys Rev Lett* 1994, 72(3):416–419.
26. Bol AA, Meijerink A. Long-lived Mn^{2+} emission in nanocrystalline ZnS:Mn^{2+}. *Phys Rev A Gen Phys* 1998, 58(24):15997–16000.
27. Murase N, Jagannathan R, Kanematsu Y, Watanabe M, Kurita A, et al. Fluorescence and EPR characteristics of Mn^{2+}-Doped ZnS nanocrystals prepared by aqueous colloidal method. *J Phys Chem B* 1999, 103(5):754–760.
28. Bryan JD, Gamelin DR. In: Karlin KD. eds. *Progress in Inorganic Chemistry*. New York: John Wiley & Sons; 2005, 47–126.
29. Yu I, Isobe T, Senna M. Optical properties and characteristics of ZnS nano-particles with homogeneous Mn distribution. *J Phys Chem Solids* 1996, 57(4):373–379.
30. Murray CB, Norris DJ, Bawendi MG. Synthesis and characterization of nearly monodisperse CdE (E = sulfur, selenium, tellurium) semiconductor nanocrystallites. *J Am Chem Soc* 1993, 115(19):8706–8715.
31. Norris DJ, Yao N, Charnock FT, Kennedy TA. High-quality manganese-doped ZnSe nanocrystals. *Nano Lett* 2001, 1(1):3–7.
32. Suyver JF, Wuister SF, Kelly JJ, Meijerink A. Luminescence of nanocrystalline ZnSe:Mn^{2+}. *Phys Chem Chem Phys* 2000, 2(23):5445–5448.
33. Erwin SC, Zu L, Haftel MI, Efros AL, Kennedy TA, et al. Doping semiconductor nanocrystals. *Nature* 2005, 436(7047):91–94.
34. Hanif KM, Meulenberg RW, Strouse GF. Magnetic ordering in doped $Cd^{1-x}Co^{x}Se$ diluted magnetic quantum dots. *J Am Chem Soc* 2002, 124(38):11495–11502.
35. Archer PI, Santangelo SA, Gamelin DR. Direct observation of sp-d exchange interactions in colloidal Mn^{2+}- and Co^{2+}-doped CdSe quantum dots. *Nano Lett* 2007, 7(4):1037–1043.
36. Santra S, Yang HS, Holloway PH, Stanley JT, Mericle RA. Synthesis of water-dispersible fluorescent, radio-opaque, and paramagnetic CdS:Mn/ZnS quantum dots: a multifunctional probe for bioimaging. *J Am Chem Soc* 2005, 127(6):1656–1657.
37. Wang S, Jarrett BR, Kauzlarich SM, Louie AY. Core/shell quantum dots with high relaxivity and photoluminescence for multimodality imaging. *J Am Chem Soc* 2007, 129(13):3848–3856.

38. Zhang X, Brynda M, Britt RD, Carroll EC, Larsen DS, et al. Synthesis and characterization of manganese-doped silicon nanoparticles: Bifunctional paramagnetic-optical nanomaterial. *J Am Chem Soc* 2007, 129(35):10668–10669.

39. Norberg NS, Kittilstved KR, Amonette JE, Kukkadapu RK, Schwartz DA, et al. Synthesis of colloidal Mn^{2+}:ZnO quantum dots and high-T_C ferromagnetic nanocrystalline thin films. *J Am Chem Soc* 2004, 126(30):9387–9398.

40. Yi DK, Selvan ST, Lee SS, Papaefthymiou GC, Kundaliya D, et al. Silica-coated nanocomposites of magnetic nanoparticles and quantum dots. *J Am Chem Soc* 2005, 127(14):4990–4991.

41. Osseo-Asare K, Arriagada FJ. Preparation of SiO_2 nanoparticles in a nonionic reverse micellar system. *Colloids Surf* 1990, 50:321–339.

42. Darbandi M, Thomann R, Nann T. Single quantum dots in silica spheres by microemulsion synthesis. *Chem Mater* 2005, 17(23):5720–5725.

43. Koole R, van Schooneveld MM, Hilhorst J, de Mello Donega C, Hart DCt, et al. On the incorporation mechanism of hydrophobic quantum dots in silica spheres by a reverse microemulsion method. *Chem Mater* 2008, 20(7):2503–2512.

44. Kim J, Lee JE, Lee J, Yu JH, Kim BC, et al. Magnetic fluorescent delivery vehicle using uniform mesoporous silica spheres embedded with monodisperse magnetic and semiconductor nanocrystals. *J Am Chem Soc* 2006, 128(3):688–689.

45. Salgueirino-Maceira V, Correa-Duarte MA, Spasova M, Liz-Marzan LM, Farle M. Composite silica spheres with magnetic and luminescent functionalities. *Adv Funct Mater* 2006, 16(4):509–514.

46. Kim J, Lee JE, Lee J, Jang Y, Kim SW, et al. Generalized fabrication of multifunctional nanoparticle assemblies on silica spheres. *Angew Chem Int Ed Engl* 2006, 45(29):4789–4793.

47. Stöber W, Fink A, Bohn E. Controlled growth of monodisperse silica spheres in the micron size range. *J Colloid Interface Sci* 1968, 26:62–69.

48. Lewin M, Carlesso N, Tung CH, Tang XW, Cory D, et al. Tat peptide-derivatized magnetic nanoparticles allow in vivo tracking and recovery of progenitor cells. *Nat Biotechnol* 2000, 18(4):410–414.

49. Miltenyi S, Müller W, Weichel W, Radbruch A. High gradient magnetic cell separation with MACS. *Cytometry* 1990, 11(2):231–238.

50. Molday RS, Yen SPS, Rembaum A. Application of magnetic microspheres in labelling and separation of cells. *Nature* 1977, 268(5619):437–438.

51. Sathe TR, Agrawal A, Nie SM. Mesoporous silica beads embedded with semiconductor quantum dots and iron oxide nanocrystals: Dual-function microcarriers for optical encoding and magnetic separation. *Anal Chem* 2006, 78(16):5627–5632.

52. Gaponik N, Radtchenko IL, Sukhorukov GB, Rogach AL. Luminescent polymer microcapsules addressable by a magnetic field. *Langmuir* 2004, 20(4):1449–1452.

53. Xie HY, Zuo C, Liu Y, Zhang ZL, Pang DW, et al. Cell-targeting multifunctional nanospheres with both fluorescence and magnetism. *Small* 2005, 1(5):506–509.

54. Hong X, Li J, Wang MJ, Xu JJ, Guo W, et al. Fabrication of magnetic luminescent nanocomposites by a layer-by-layer self-assembly approach. *Chem Mater* 2004, 16(21):4022–4027.

55. Caruso F. Nanoengineering of particle surfaces. *Adv Mater* 2001, 13(1):11–22.

56. Sukhorukov GB, Rogach AL, Garstka M, Springer S, Parak WJ, et al. Multifunctionalized polymer microcapsules: Novel tools for biological and pharmacological applications. *Small* 2007, 3(6):944–955.

57. Xu HX, Sha MY, Wong EY, Uphoff J, Xu YH, et al. Multiplexed SNP genotyping using the Qbead (TM) system: a quantum dot-encoded microsphere-based assay. *Nucleic Acids Res* 2003, 31(8):e431–e4310.

58. Frullano L, Meade TJ. Multimodal MRI contrast agents. *J Biol Inorg Chem* 2007, 12(7):939–949.

59. Modo M, Cash D, Mellodew K, Williams SCR, Fraser SE, et al. Tracking transplanted stem cell migration using bifunctional, contrast agent-enhanced, magnetic resonance imaging. *Neuroimage* 2002, 17(2):803–811.

60. Huber MM, Staubli AB, Kustedjo K, Gray MHB, Shih J, et al. Fluorescently detectable magnetic resonance imaging agents. *Bioconjug Chem* 1998, 9(2):242–249.

61. Mulder WJM, Strijkers GJ, van Tilborg GAF, Griffioen AW, Nicolay K. Lipid-based nanoparticles for contrast-enhanced MRI and molecular imaging. *NMR Biomed* 2006, 19(1):142–164.

62. Pierre VC, Botta M, Raymond KN. Dendrimeric gadolinium chelate with fast water exchange and high relaxivity at high magnetic field strength. *J Am Chem Soc* 2005, 127(2):504–505.

63. van Tilborg GAF, Mulder WJM, Chin PTK, Storm G, Reutelingsperger CP, et al. Annexin A5-conjugated quantum dots with a paramagnetic lipidic coating for the multimodal detection of apoptotic cells. *Bioconjug Chem* 2006, 17(4):865–868.

64. Mulder WJ, Castermans K, Lowik CW, Kaijzel GJ, Strijkers GJ, et al. Parallel intravital microscopy, MR imaging, and fluorescence imaging of tumor angiogenesis using paramagnetic quantum dots. *Presented at Joint Annual Meeting ISMRM-ESMRMB*, Berlin, 2007.

65. Prinzen L, Miserus RJJHM, Dirksen A, Hackeng TM, Deckers N, et al. Optical and magnetic resonance imaging of cell death and platelet activation using annexin A5-functionalized quantum dots. *Nano Lett* 2007, 7(1):93–100.
66. Yang HS, Santra S, Walter GA, Holloway PH. Gd-III-functionalized fluorescent quantum dots as multimodal imaging probes. *Adv Mater* 2006, 18(21):2890–2894.
67. Gerion D, Herberg J, Bok R, Gjersing E, Ramon E, et al. Paramagnetic silica-coated nanocrystals as an advanced MRI contrast agent. *J Biochem Mol Biol Biophys* 2007, 111(34):12542–12551.
68. Ersoy H, Rybicki FJ. Biochemical safety profiles of gadolinium-based extracellular contrast agents and nephrogenic systemic fibrosis. *J Magn Reson Imaging* 2007, 26(5):1190–1197.
69. Soo Choi H, Liu W, Misra P, Tanaka E, Zimmer JP, et al. Renal clearance of quantum dots. *Nat Biotechnol* 2007, 25(10):1165–1170.
70. Derfus AM, Chan WCW, Bhatia SN. Probing the cytotoxicity of semiconductor quantum dots. *Nano Lett* 2004, 4(1):11–18.
71. Kirchner C, Liedl T, Kudera S, Pellegrino T, Javier AM, et al. Cytotoxicity of colloidal CdSe and CdSe/ZnS nanoparticles. *Nano Lett* 2005, 5(2):331–338.
72. Lewinski N, Colvin V, Drezek R. Cytotoxicity of nanoparticles. *Small* 2008, 4(1):26–49.
73. Hardman R. A toxicologic review of quantum dots: toxicity depends on physicochemical and environmental factors. *Environ Health Perspect* 2006, 114(2):165–172.
74. Klostranec JM, Chan WCW. Quantum dots in biological and biomedical research: recent progress and present challenges. *Adv Mater* 2006, 18(15):1953–1964.

